A simple method to measure the temperature and levitation height of devices rotating at cryogenic temperatures

Paolo de Bernardis,[1,2] Fabio Columbro,[1,2] Silvia Masi,[1,2,a)] Alessandro Paiella,[1,2] and Giovanni Romeo[3]
[1)] *Dipartimento di Fisica, Sapienza Universitá di Roma, Italy*
[2)] *INFN, Sezione di Roma, Italy*
[3)] *Istituto Nazionale di Geofisica e Vulcanologia, Roma, Italy*

(Dated: 20 February 2020)

We describe a simple system to measure the temperature and levitation height of levitating cryogenic devices in rotation. Devices of this kind are the half-wave-plates (HWP) rotating on superconductive magnetic bearings used in several cryogenic polarimeters for the Cosmic Microwave background (CMB). The temperature measurement is important to monitor the radiative background and potential systematic effects in the polarimeter. In our implementation, the temperature sensor is a thermistor, physically mounted on the rotating device. The sensor is biased with an AC current, which is transferred from the steady electronics to the rotating device via capacitive coupling. The levitation height sensor is a network of capacitors, similar to the one used for the capacitive coupling of the thermistor. We describe the optimization of the readout system and its performance, which has been tested on a room-temperature prototype. We show that this system reaches an accuracy better than 3% for the measurement of the thermistor resistance, and an accuracy of $\sim 10\,\mu$m for the measurement of its levitation height.

I. INTRODUCTION

Modern measurements of Cosmic Microwave Background (CMB) polarization[1] use large-throughput arrays of Transition Edge Sensors[2] or Kinetic Inductance detectors[3–6] operating in a cryogenic environment. The detectors are cooled at sub-K temperature to maximize their sensitivity, and the optical components of the polarimeter are also cooled to reduce the radiative loading on the detectors, and minimize systematic effects. A Stokes polarimeter uses a rotating HWP and a polarizer to modulate the linearly polarized component. The HWP temperature should also be minimized (see[7,8] for a discussion): this is very important in particular in space-based experiments, where the radiative background from the sky is very low. Superconductive magnetic bearings provide a nearly frictionless, fast rotation of the HWP, perfectly compatible with the cryogenic implementation of the Stokes polarimeter[9–12]. The HWP assembly levitates and rotates in the magnetic field produced by the interaction of a permanent magnet in the rotor and a set of static superconductive bulks, reaching a mechanical rotation speed $f_o \sim$ a few Hz, and modulating the polarized signal at $\sim 4 f_o$.

In this configuration, however, there is no mechanical contact between the HWP and the rest of the system. Any power dissipation (for example due to eddy currents) or power absorbed (for example due to the radiative load from the external environment) raises the temperature of the rotating assembly and the HWP, which can cool-down only radiatively. At low temperatures, radiative cooling is not effective, so the power dissipation on the rotor should be carefully minimized. In Fig. 1 we show the results of a simulation of the temperature of a rotating HWP of this kind. It is evident that small power inputs can produce a temperature raise from few K to tens of K, resulting in increased radiative load on the detectors and increased spurious synchronous signals.

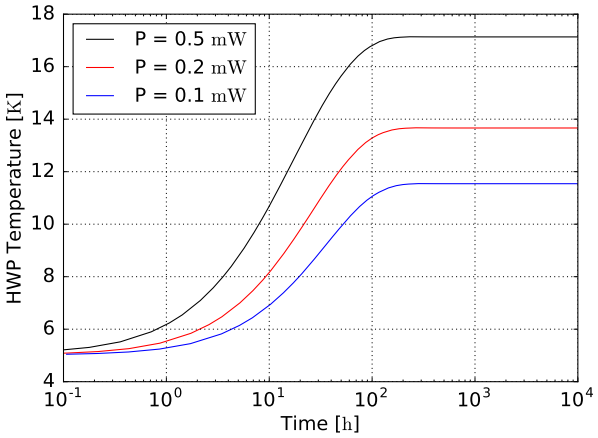

FIG. 1. Simulation of the temperature of a levitating rotating metal-mesh HWP (300 mm diameter, which is the range of interest for the HWP of the LiteBIRD experiment[13,14]), radiatively heated with 3 different levels of input power, starting from a base temperature of 5 K.

For this reason it is very important to monitor the temperature of the HWP, using precise measurements. In the case of a contactless rotor, one way to measure the temperature of the HWP is by monitoring its thermal emission. To this purpose, the side of the rotating assembly facing the internal part of the cryogenic system is blackened, so that its thermal emission radiatively cools the rotating assembly, and can be measured by a far-IR/mm-wave detector. The signal detected with a reasonable

[a)] silvia.masi@roma1.infn.it

throughput ($0.2\,\mathrm{cm}^2\,\mathrm{sr}$) and optical bandwidth (20%) at a sensing wavelength of 1.4 mm is in the 1 pW to 100 pW range, for temperatures between 3 K and 20 K. For a precision measurement, sensitive detectors and a chopping mechanism to alternate the black surface and a reference cold blackbody, especially at the lowest edge ($\sim 2\,\mathrm{K}$) of the temperature range, are required.

Here we describe a simpler, cost effective, reliable method to measure the temperature of the rotating assembly, avoiding the use of such a complex detection system. This is based on a regular thermistor, mounted on the rotating assembly. The thermistor is capacitively coupled to the steady readout system, and biased with an AC current. A simple extension of the method also allows for monitoring the distance of the rotor with respect of the stator along the rotation axis. In the following we describe the measurement system, its optimization, and its performance.

II. THE CAPACITIVELY COUPLED THERMISTOR

A. Practical implementation

The block diagram of the system is shown in Fig. 2. A regular thermistor for cryogenic temperature measurements (RuO_2 resistor, or CERNOX^{TM15}, or similar, with resistance values ranging between $500\,\Omega$ and $50\,\mathrm{k}\Omega$) is mounted on the rotary assembly. Each contact of the thermistor is connected to one pole of a plane capacitor, *i.e.* a simple rectangular copper pad, say $10\,\mathrm{mm}\times 50\,\mathrm{mm}$, mounted on the rotating assembly. The other pole of the same capacitor is similar, and is mounted on the stator. At a certain angle of the rotation of the HWP, the two poles of both capacitors will align one on top of the other, with a gap of $\sim 1\,\mathrm{mm}$ between the poles, thus creating two capacitors (with capacitance $2C \sim 2\,\mathrm{pF}$ each). The steady pole of the first capacitor is connected to an AC voltage generator, while the steady pole of the second capacitor is connected to a low-value load resistor ($R_L \sim 50\,\Omega$) closing the circuit on the ground. When the poles are aligned, an AC current flows through the thermistor, with an intensity depending on its resistance R, which in turn depends on its temperature ($R = R(T)$).

B. Basic circuit analysis and optimization

The equivalent circuit of the capacitively coupled thermistor is reported in Fig. 3.

The transfer function for the circuit in Fig. 3 can be written:

$$\frac{\Delta V_{out}}{\Delta V_{in}} = \frac{1}{1+\frac{Z}{R_L}} \tag{1}$$

where Z is the combined impedance of the network of

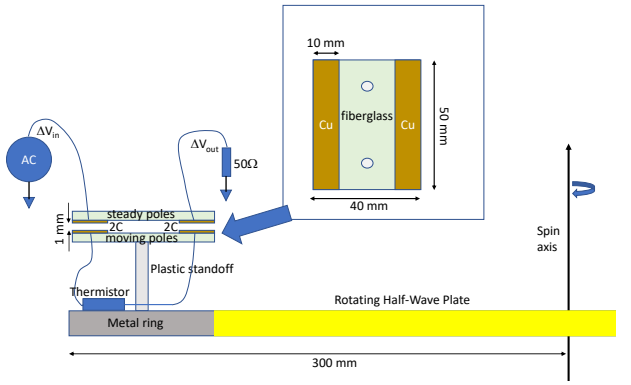

FIG. 2. Schematic diagram of the temperature measurement.

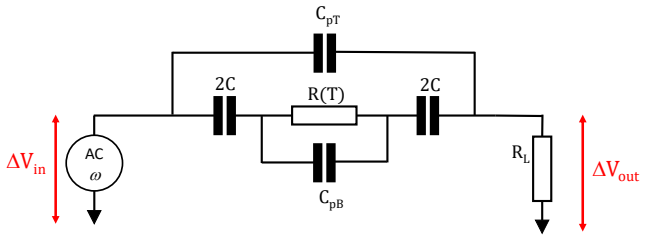

FIG. 3. Equivalent circuit of the temperature measurement. The excitation ΔV_{in} is produced by a voltage generator at frequency $f = 2\pi\omega$. The rotating capacitors have capacitance $2C \sim 2\,\mathrm{pF}$; the thermistor has resistance $R(T)$ in the kΩ to several tens of kΩ range; $C_{pT} \sim 0.3\,\mathrm{pF}$ is the parasitic capacitance between the steady poles of the two capacitors, while $C_{pB} \sim 0.3\,\mathrm{pF}$ is the parasitic capacitance between the rotating poles of the two capacitors; $R_L \sim 50\,\Omega$ is the load resistor.

horizontal components in Fig.3 :

$$\mathrm{Re}\,(Z) = \frac{R\,(T)}{\left(1+C_{pT}/C\right)^2+\omega^2R^2\,(T)\,C_p^2} \tag{2}$$

$$\mathrm{Im}\,(Z) = \frac{1}{\omega C}\frac{\left(1+C_{pT}/C\right)+\omega^2R^2\,(T)\,(C+C_{pB})\,C_p}{\left(1+C_{pT}/C\right)^2+\omega^2R^2\,(T)\,C_p^2} \tag{3}$$

$$C_p = C_{pB}(1+C_{pT}/C)+C_{pT}. \tag{4}$$

The modulus and phase of the transfer function are plotted in Fig. 4, for the components values listed in the caption of Fig. 3.

From Fig. 4 is evident that, for the typical values of the components considered here, the optimal excitation frequency is in the 20–50 MHz range, where the output signal excursion is significant and roughly equalized.

The expected non-linear relation between the resistance of the thermistor and the output signal is shown in Fig. 5.

With an excitation amplitude of $1\,\mathrm{V_{rms}}$, the output signal is in the range of several tens of $\mathrm{mV_{rms}}$. However, in the range of temperatures of interest here, the

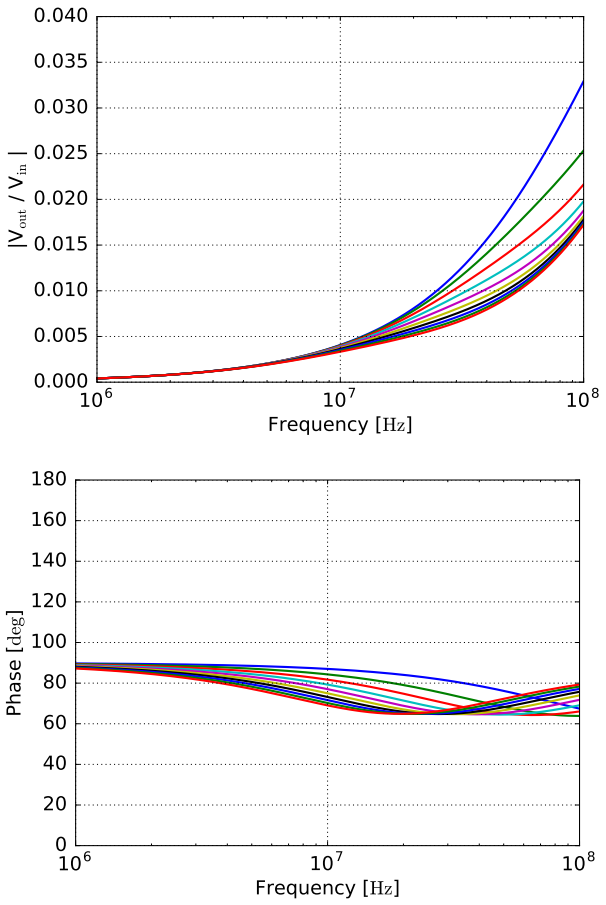

FIG. 4. Modulus (top) and Phase shift (bottom) of the transfer function of the readout circuit, for thermistor values between 1 kΩ (top line) and 10 kΩ (bottom line).

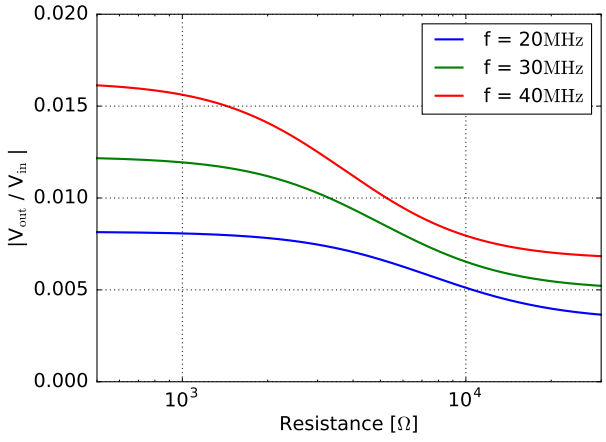

FIG. 5. Expected output voltage as a function of the thermistor resistance, for excitation frequencies $f = 20, 30, 40$ MHz (bottom to top lines).

rms voltage across the thermistor must be limited below 0.01 V_{rms}, to avoid self-heating of the thermistor. This requires an excitation amplitude of the capacitors-thermistor network smaller than 1 V_{rms}, as shown in Fig. 6, and results in very small (order of 0.1 mV_{rms}) output signals across the load resistor of Fig. 3.

For this reason, a custom readout scheme has been developed, as described below.

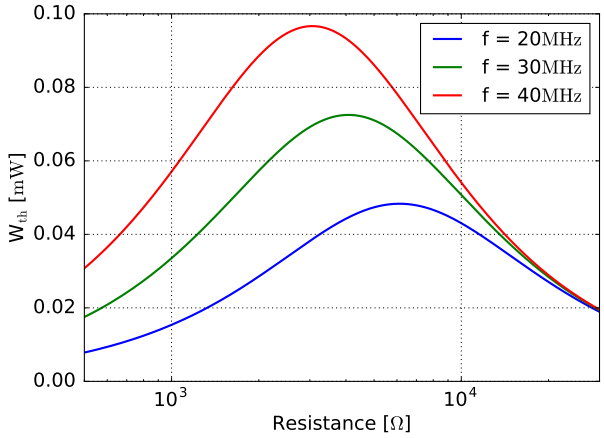

FIG. 6. Expected power dissipated in the thermistor, as a function of the thermistor resistance, for excitation frequencies $f = 20, 30, 40$ MHz (bottom to top lines), for a 1 V_{rms} excitation amplitude. The power scales as the square of the excitation voltage, and must be reduced to avoid self-heating of the thermistor.

C. Excitation and readout circuit

In the simplest implementation, the excitation signal is obtained from a $f = 25$ MHz digital clock, which is filtered by a resonant circuit to obtain a sine-wave excitation. We prefer to remove the higher harmonics present in the original square-wave, since they produce large spikes through the thermistor-capacitors network of Fig. 3, which are difficult to model due to the presence of stray capacitance and uncertainties in the high frequency gain of the active components in the following signal recovery chain. This sine-wave signal is reduced in amplitude by means of a −20 dB attenuator, to obtain the excitation signal ΔV_{in}, and connected via a 50 Ω, 2 m long stainless steel coax to the thermistor-capacitors network. This results in an excitation across the thermistor $\Delta V_{th} \sim 10$ mV_{rms}. The signal across the load resistor is connected via a 50 Ω, 2 m long coax to the input of a low-noise amplifier, based on a MAR-8 MMIC module, with gain ∼ 30 dB. The output is low-pass filtered, and sent to an RF-to-rms converter based on an AD8361 chip. The DC output of the AD8361 is amplified by a factor 10 and digitized.

A second RF-to-rms converter is used to monitor any change of the excitation amplitude.

The block-diagram of the readout electronics is visible in Fig. 7.

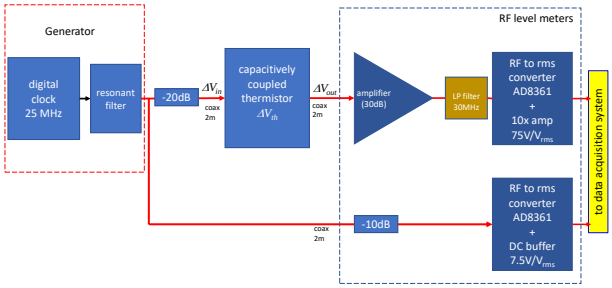

FIG. 7. Block-diagram of the simplest excitation and readout scheme.

The output of this readout circuit has a significant offset, due to the parasitic capacitance and the rms value of the noise of the thermistor and amplifier, but is usable anyway if the noise level is stable (*i.e.* if external noise and RFI sources do not couple significantly to the capacitors-thermistor network).

In Fig. 8 we plot the measured response of the readout circuit to different values of the thermistor resistance.

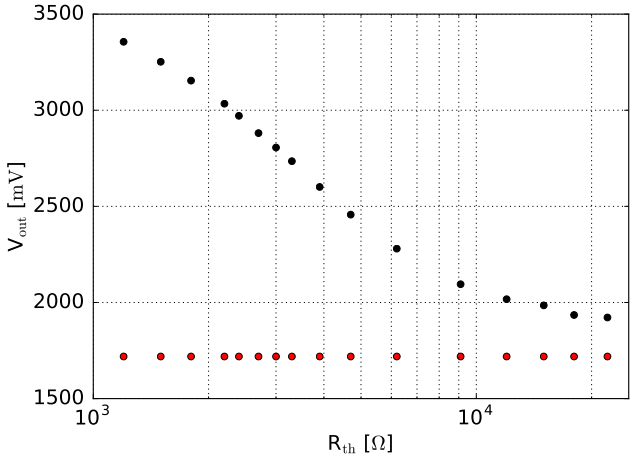

FIG. 8. Measured response of the readout circuit shown in Fig. 7 to different values of the thermistor resistance (black dots). The red dots represent the measured values of the excitation monitor output. If the thermistor is a CERNOX^{TM} model CX-1050, resistance values between 1 kΩ and 10 kΩ correspond to temperatures between ∼10 K and ∼2 K, which is the range of interest for the HWP of the LSPE[16] and QUBIC[17] experiments.

The output noise of the readout circuit depends on the Johnson noise of the thermistor, on the noise of the amplifier, and on the electromagnetic interference on the capacitive sensor. For a 50 Ω load resistor, the Johnson voltage noise is $\sqrt{4k_BTR} \sim 1\,\mathrm{nV}/\sqrt{\mathrm{Hz}}$. Given the small value of the source resistance, the current noise of the amplifier is negligible, while the voltage noise of the amplifier is $\sim 1\,\mathrm{nV}/\sqrt{\mathrm{Hz}}$. Over a bandwidth $\Delta f \sim 30\,\mathrm{MHz}$, with a gain $G \sim 30$, the standard deviation of the output of the amplifier is $RMS \sim 0.2\,\mathrm{mV_{rms}}$. The RF to rms converter operates with a time constant $\tau \sim 20\,\mu\mathrm{s}$, with a gain $G_c \sim 7.5\,\mathrm{V/V_{rms}}$, and an additional gain $G_a = 10$ is provided by the output amplifier. The minimum fluctuation of the output of the readout circuit is thus $\sigma_{out} = G_c G_a \times RMS/\sqrt{2\tau\Delta f} \sim 0.5\,\mathrm{mV_{rms}}$.

The average value of the output due to the bias signal, instead, is of the order of several hundreds of $\mathrm{mV_{rms}}$ to $\sim 2\,\mathrm{V_{rms}}$, thus resulting in an expected signal-to-noise ratio much larger than 100, if interference is negligible.

We have tested the previous forecast acquiring the output of the readout with a 24-bit A/D converter. The measured *rms* fluctuation is consistent with the expected value when the capacitor network is well shielded in a grounded metal box. Such a configuration is representative of the operation of the sensor inside the metal cryostat of a CMB polarimeter.

When operated in the laboratory, outside the metal shielding, the system is sensitive to the position with respect to the rotator and the environment, and also to cell-phones and computer-generated EMI. These effects limit the performance of the system in the measurements reported below, which, however, reach anyway an acceptable performance level.

Improved performance of the readout, and reduced sensitivity to EMI, might be obtained by reducing the bandwidth at the amplifier output (*e.g.* replacing the low-pass filter in Fig. 7 with a resonant filter. In order to avoid thermally driven mismatches between the fiter response and the generator frequency, a lock-in demodulation might be used. We leave this to future developments, since even for the simple readout circuit described above the readout noise is not the limiting factor, as we show below.

III. MEASURED PERFORMANCE

We tested the performance of the measurement method using a room-temperature mock-up, where the levitating rotor is replaced by a 500 mm diameter disk rotating on a low-friction ball-bearing, and the thermistor has been simulated using resistors with values spanning the expected range $R_{th} \sim 1\,\mathrm{k\Omega} - 30\,\mathrm{k\Omega}$. The rotor driver, based on steady coils pushing or pulling on permanent magnets on the disk, and the strong levitation magnet of the superconducting magnetic bearing are the same as for the cryogenic device.

The capacitance $2C$ of the thermistor readout network depends on the distance between the steady and moving capacitor poles. In case a superconductive magnetic bearing is used to levitate the rotating device, small fluctuations of the distance between the poles are possible.

These must and can be monitored adding an identical capacitive network on the side of each thermistor readout network. In these additional *reference* networks, the thermistors are replaced by metal wires with negligible resistance. During the rotation of the device, the steady capacitor poles will face sequentially the poles of each thermistor network and its reference network, so the output of the readout chain will monitor in close sequence the thermistor resistance and the distance between the poles.

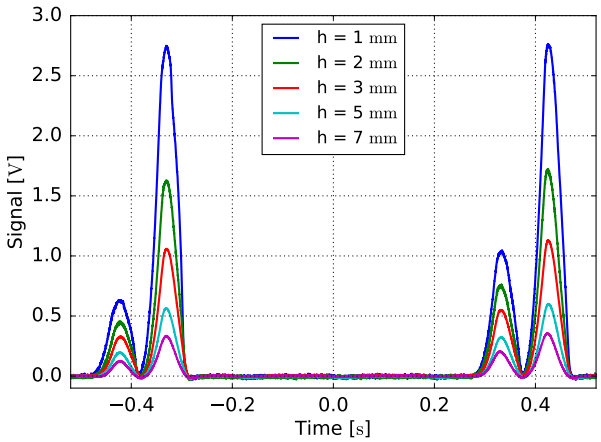

FIG. 9. Sample records of the readout output while the rotor was spinning at 40 rpm. The four peaks (left to right) correspond to the first thermistor network (R_{th}=10 kΩ), its reference capacitor, a second thermistor network (R_{th}=4.7 kΩ), its reference capacitor. The reference capacitors provide an effective way to estimate the distance between the capacitor poles, which depends on the vertical position of the levitating rotor.

In Fig. 9 we report sample records of the raw readout output when two thermistors with resistances of 10 kΩ and 4.7 kΩ, spaced by 180° in azimuth, are mounted on the rotor. Each thermistor network is followed by its *reference* network. The measurement has been repeated for different values of the distance h between the moving capacitors poles and the steady capacitor poles, while the rotor is spinning at ~ 40 rpm.

The data demonstrate that the reference capacitor networks allow for a good measurement of the distance between the poles. If we assume a distance between the capacitor poles of 1 mm, the system has a resolution $dV/dh \sim 1.6\,\mathrm{V\,mm^{-1}}$ while for a distance of 2 mm the resolution is $dV/dh \sim 0.75\,\mathrm{V\,mm^{-1}}$.

The distance measurements can thus be used to correct the effect of distance fluctuations in the measurements of the thermistor resistance. In order to check the effectiveness of the method, we normalize the peak signal of each thermistors network to the peak signal of the its reference network, and plot in Fig. 10 the ratio of these ratios. Regardless of the distance between the capacitor poles, the ratio remains approximately constant, confirming the effectiveness of the correction method.

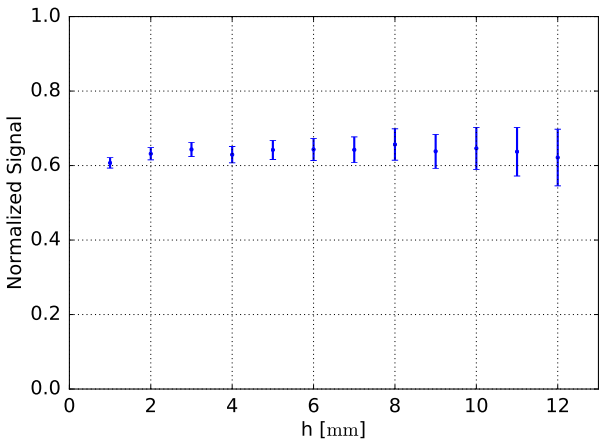

FIG. 10. Ratio between the peak signals of two thermistor networks (R_{th} =4.7 kΩ and R_{th} =10 kΩ), each normalized to the peak signal of its reference network, plotted for a wide range of distances between steady and moving capacitor poles.

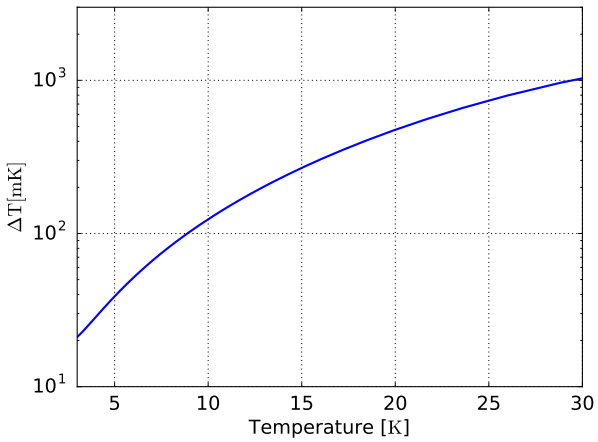

FIG. 11. Error on the measured temperature, estimated for a CX-1050 sensor read through the readout circuit described in the text.

Note that the measured *rms* fluctuation of the readout output σ_M is several $\mathrm{mV_{rms}}$, larger than the one expected from Johnson and amplifier noise alone. This means that significant perturbations arise from the unshielded operation, and the stray capacitance variations with respect to the surrounding environment.

The measured output signal noise σ_M is readily converted into an error in the temperature measurement, once the $R_{th}(T)$ characteristic of the thermistor is defined:

$$\Delta T = \frac{dT}{dR}\sigma_R = \frac{dT}{dR}\frac{dR}{dV}\sigma_M \qquad (5)$$

where the first derivative is estimated from the calibration curve of the thermistor $R_{th}(T)$, while the second derivative is estimated from the calibration data $V(R_{th})$ of Fig.8. In Fig. 10 we plot ΔT for a CERNOX$^{\mathrm{TM}}$ CX-

1050 temperature sensor. Since the measured σ_M does not depend on the value of the thermistor resistance, the behaviour of ΔT versus rotor temperature is due to the combination of the thermistor resistance $R_{th}(T)$ becoming steeper for lower temperatures, and the $V(R_{th})$ of the readout circuit mildly decreasing for the correspondingly larger resistances. The relative error remains anyway always smaller than 3%, in the entire temperature range of interest.

Using the measured noise, we can also compute the error in the measurement of the levitation height:

$$\sigma_h = \frac{dV}{dh}\sigma_M. \quad (6)$$

We find that variations of the height as small as $\sigma_h \sim 6\,\mu\text{m}$ and $\sigma_h \sim 13\,\mu\text{m}$, for distances h of 1 mm and 2 mm respectively, can be detected reading the reference capacitive networks.

Note that, in principle, any tilt of the rotor could be sampled by replicating 3 measurement assemblies, separated by 120° in azimuth.

IV. CONCLUSIONS

We have designed, built and tested a device able to sense the temperature and the position of a levitating rotor during its fast rotation at cryogenic temperature. The measurement is based on regular thermistors, mounted on the rotor, periodically and briefly biased by a high-frequency AC current, through a capacitive network.

We have demonstrated the correct operation of the capacitive readout in a room-temperature real-world environment, including the electromagnetic interference of the rotor driver coils and of the levitation magnet, and even variable capacitive coupling to the surrounding environment, which will arguably be absent in the cryogenic operation inside a grounded cryostat shell. The presence of varying capacitive coupling towards the surrounding environment results in increased output fluctuations, with respect to the ones due to resistors and amplifier noise, but the resulting total noise is sufficiently small to warrant good measurements of the temperature. An alternative inductive coupling between the rotating thermistor and the static readout system, while in principle possible and effective, would be severely affected by the magnetic interference from the driving coils.

We do not expect any change in the performance of the measurement setup when cooled at cryogenic temperatures. The coaxial cables we have used have the same dimensions and length which will be used in the cryogenic setup, and we do not use any electronic component near the capacitive networks, which are intrinsically temperature-independent.

Using a CX-1050 CERNOX$^{\text{TM}}$ thermistor, the error in the measured resistance converts into an error in the temperature smaller than 3%, for the $2 - 30\,\text{K}$ temperature range of interest for the levitating HWPs of cryogenic CMB polarimeters.

Reference capacitive networks read through the same circuit allow for precision measurements of the levitation height of the rotor, with a resolution of $\sim 10\,\mu\text{m}$. This provides an important diagnostic of the dynamics of the rotor, and allows for corrections of the thermistor resistance measurement fluctuations due to any variation of levitation height.

ACKNOWLEDGMENTS

This research has been supported by the Italian Space Agency (ASI-LSPE and LiteBIRD contracts) and by the Italian National Institute for Nuclear Physics (INFN-LSPE activity).

[1] D. Baumann and H. V. Peiris, Adv.Sci.Lett. **2**, 105 (2009).
[2] F. Columbro, P. G. Madonia, L. Lamagna, E. S. Battistelli, A. Coppolecchia, P. de Bernardis, R. Gualtieri, S. Masi, A. Paiella, F. Piacentini, G. Presta, M. Biasotti, G. D'Alessandro, F. Gatti, L. Mele, and B. Siri, Journal of Low Temperature Physics (2020).
[3] P. A. R. Ade *et al.*, The Astrophysical Journal **812**, 176 (2015).
[4] H. McCarrick *et al.*, *A&A* **610**, A45 (2018).
[5] S. Masi *et al.*, Journal of Cosmology and Astroparticle Physics **2019** (7), 003.
[6] A. Paiella, A. Coppolecchia, L. Lamagna, P. A. R. Ade, E. S. Battistelli, M. G. Castellano, I. Colantoni, F. Columbro, G. D'Alessandro, P. de Bernardis, S. Gordon, S. Masi, P. Mauskopf, G. Pettinari, F. Piacentini, G. Pisano, G. Presta, and C. Tucker, Journal of Cosmology and Astroparticle Physics **2019** (1), 039, arXiv:1810.00598 [astro-ph.IM].
[7] M. Salatino, P. de Bernardis, and S. Masi, *A&A* **528**, 1 (2011).
[8] F. Columbro, E. S. Battistelli, A. Coppolecchia, G. D'Alessandro, P. de Bernardis, L. Lamagna, S. Masi, L. Pagano, A. Paiella, F. Piacentini, and G. Presta, Astronomische Nachrichten **340**, 83 (2019), arXiv:1904.01891 [astro-ph.IM].
[9] T. Essinger-Hileman, A. Kusaka, *et al.*, Review of Scientific Instruments **87** (2016).
[10] B. R. Johnson, F. Columbro, D. Araujo, M. Limon, B. Smiley, G. Jones, B. Reichborn-Kjennerud, A. Miller, and S. Gupta, Review of Scientific Instruments **88**, 105102 (2017), https://doi.org/10.1063/1.4990884.
[11] F. Columbro, P. de Bernardis, and S. Masi, Review of Scientific Instruments **89** (2018).
[12] Y. Sakurai, T. Matsumura, T. Iida, H. Kanai, N. Katayama, H. Imada, H. Ohsaki, Y. Terao, T. Shimomura, H. Sugai, H. Kataza, R. Yamamoto, and S. Utsunomiya, IEEE Transactions on Applied Superconductivity **28**, 2797302 (2018).
[13] Y. Sekimoto, P. Ade, K. Arnold, *et al.*, in *Space Telescopes and Instrumentation 2018: Optical, Infrared, and Millimeter Wave*, Society of Photo-Optical Instrumentation Engineers (SPIE) Conference Series, Vol. 10698 (2018) p. 106981Y.
[14] H. Sugai, P. A. R. Ade, Y. Akiba, *et al.*, Journal of Low Temperature Physics , 35 (2020), arXiv:2001.01724 [astro-ph.IM].
[15] CERNOX$^{\text{TM}}$ is a trademark of Lake Shore Cryotronics, Inc.
[16] F. Lamagna *et al.*, Journal of Low Temperature Physics (2020).
[17] F. Mele and QUBIC Collaboration, Proceedings of the 10th YRM (2020).